Supporting information for

Multi-functional molecule advancing the efficiency of pure 3D $FASnI_3$ perovskite solar cells based on tin tetraiodide reduction method

Hao Li,[1†] Haoyu Shi,[1†] Qin Tan,[1] Guocong Chen,[1] Jiafeng Wang,[1] Guoqiang Ma,[1] Dong He,[1] Tianle Cheng,[1] Han Gao,[1] Francesco Lamberti,[2] Zhubing He[1,*]

[1] Department of Materials Science and Engineering, Institute of Innovative Materials (I2M), Shenzhen Key Laboratory of Full Spectral Solar Electricity Generation (FSSEG), Southern University of Science and Technology (SUSTech), No. 1088, Xueyuan Rd., Shenzhen, 518055, Guangdong, China.

[2] Department of Chemical Sciences, University of Padova, Via Marzolo 1, 35131 Padova, Italy; Department of Industrial Engineering, University of Padova, Via Gradenigo 6a, 35131 Padova, Italy; Zhejiang Beisheng Photovoltaic Co., Ltd. No.800 Zhenbei Road, Zhili Town, Wuxing District Huzhou, Zhejiang 313000, China.

*Corresponding author. Email: hezb@sustech.edu.cn

Materials and Methods

Materials

Anhydrous solvents including N, N-dimethylformamide (DMF), dimethyl sulfoxide (DMSO), chlorobenzene (CB), isopropanol (IPA), were purchased from Sigma-Aldrich. Formamidinium iodide (FAI, 99.99%) was purchased from Great Cell Solar. Tin iodide (SnI_2, AnhydroBeads, 99.99%) was obtained from Sigma-Aldrich. Tin iodide (SnI_4, Anhydrous, 99.998%) and Phenylhydrazine-4-sulfonic acid (PHPA) were obtained from Macklin. Formamidinium Iodide (FAI) was purchased from Great Cell Solar (Australia). Bathocuproine (BCP), PCBM and ICBA were obtained from 1-Materials. UV curing sealant was purchased from Blufixx for the encapsulation process. Aluminum (Al) were obtained from commercial sources with high purity (≥99.9%).

Preparation of perovskite precursor solutions

For pristine $FASnI_3$, 137.6 mg FAI, 298.1 mg SnI_2, 13.5 mg SnF_2 and 100mg Sn powder were dissolved in 1 ml DMF and DMSO solution (volume ratio 3:1) and stirred at room temperature for 12 hours. For TTR $FASnI_3$, 137.6 mg FAI, 250.5 mg SnI_4, 13.5 mg SnF_2 and 100mg Sn powder were dissolved in 1 ml DMF and DMSO solution (volume ratio 3:1) and stirred at room temperature for 12 hours. For the PHPA solution, another 0.5-3 mg/ml PHPA was added in the preceding solution of TTR $FASnI_3$.

Device Fabrication

The patterned ITO glass substrates were cleaned using detergent, deionized water, acetone, and isopropanol in an ultrasonic bath for 20 minutes, sequentially. Then, the substrates were dried with N_2 flow and cleaned with UV-Ozone for 30 mins. After that, the PEDOT: PSS layers were deposited on the ITO glass substrates by spin-coating at 5000 rpm for 40 s, followed by post annealing at 140 °C for 10 min. The deposition of the Sn-perovskite films was performed in an N_2 glove box with the oxygen<0.1 ppm. All the precursor solutions were filtered with a 0.45 μm PTFE filter and

dropped onto PEDOT: PSS/ITO substrates, subsequently spin-coating at the speed of 5000 rpm for 60 s. All the perovskite films were treated by drop-casting 300 μL chlorobenzene as the anti-solvent during the spinning process at about 40 seconds. Then, all the films were post-annealed at 80 °C for 15 min. Then, 40 μL of ICBA or PCBM (20 mg/mL in CB) solution was spin-coated on the top of perovskite film at the speed of 1200 rpm for the 30s and annealed at 80 °C for 10 min. Finally, 5 nm BCP and 70 nm Al were evaporated on top of the film through a shadow mask by thermal evaporation. UV curable sealants with glass slides were applied to encapsulate the devices.

Film Characterizations

X-ray diffraction (XRD) spectra were collected using the Rigaku MiniFlex600 X-ray diffractometer (Cu Kα, 1.5406 Å). Top-view and cross-section morphology of the perovskite films were measured by a high-resolution field emission scanning electron microscope (SEM, TESCAM MIRA3). The absorption spectra were taken using a Shimadzu ultraviolet-visible spectrophotometer (UV-3600). Room-temperature photolunminescence (PL) spectra were measured by Spectrofluorometer (FS5, Edinburgh instruments) with 405 nm pulsed laser. X-ray photoelectron spectroscopy (XPS) measurements were carried out on an Omicron ESCA Probe XPS spectrometer (Thermo Scientific ESCALAB 250Xi). The XPS spectra were calibrated by the binding energy of 284.8 eV for C 1s. Fourier-transform infrared spectroscopy (FTIR) was measured by Fourier Transform Infrared Spectrometer (Bruker Vertex 70v) for 4000 to 400 cm^{-1}. Contact angle measurements were carried out with a KLA-Tencore D120 surface profiler. NMR spectra were recorded on Bruker Avance 500 and Bruker Avance 400 spectrometers in DMSO-d_6. The pH of the precursor solution was measured using a Rex Electric Chemical E-301-QC pH meter, which was calibrated with three standard solutions before each test.

Device Characterization

J-V measurements were carried out using a Keithley 2400 source meter in an ambient environment (roughly 20 °C and 60% relative humidity). The encapsulated devices were measured both in reverse scan (0.9 to -0.2 V, steps of 0.01 V) and forward scan (-0.2 to 0.9 V, steps of 0.01 V) with 200 ms delay time. Illumination was provided by an Oriel Sol3A solar simulator with an AM 1.5G spectrum, and light intensity of 100 mW cm^{-2} was calibrated by a standard KG-5 Si diode. The active area (0.08 cm^2) of our device was calibrated with a shadow mask during measurements. Electrochemical impedance spectroscopy and Mott-Schottky plots were conducted on the Zahner Zennium electrochemical workstation. EQE measurements for devices were carried out with an Enli-Tech EQE measurement system, and light intensity at each wavelength was calibrated with a standard single-crystal Si photovoltaic cell. Long-term operational stability was conducted with the encapsulated devices under a 1-sun-equivalent light-emitting diode lamp under an ambient environment (approximately 25 °C and 50% relative humidity). The maximum power point was recorded every 60 s. TPV and TPC measurement were carried out by 405 nm pulsed laser and oscilloscope (TDS 2024C), with frequencies set to 10Hz (TPV) and 1000Hz (TPA).

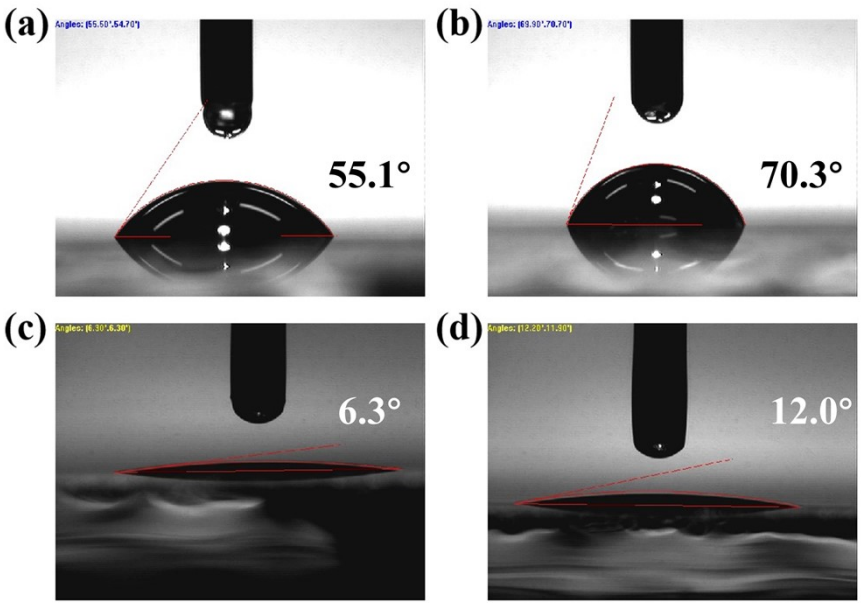

Figure S1. Perovskite film contact angle test results: (a)pristine, water. (b)TTR, water. (c)pristine, n-hexadecane. (d)TTR, n-hexadecane.

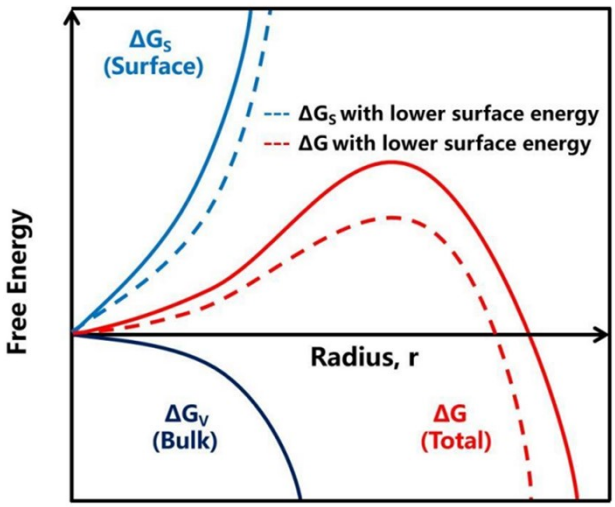

Figure S2. Schematic diagram of the classical free energy diagram for nucleation as a function of particle radius. [1]

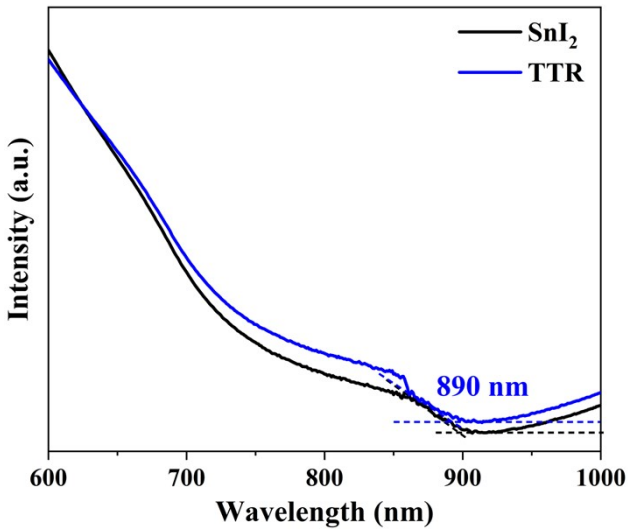

Figure S3. UV-vis absorption of pristine and TTR perovskite films.

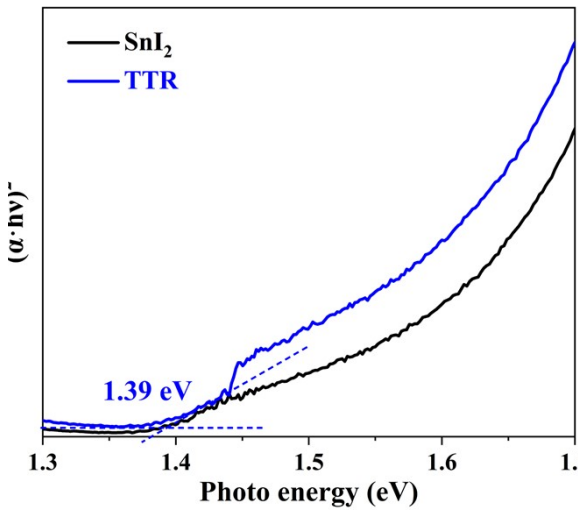

Figure S4. Tauc plot of the pristine and TTR perovskite films.

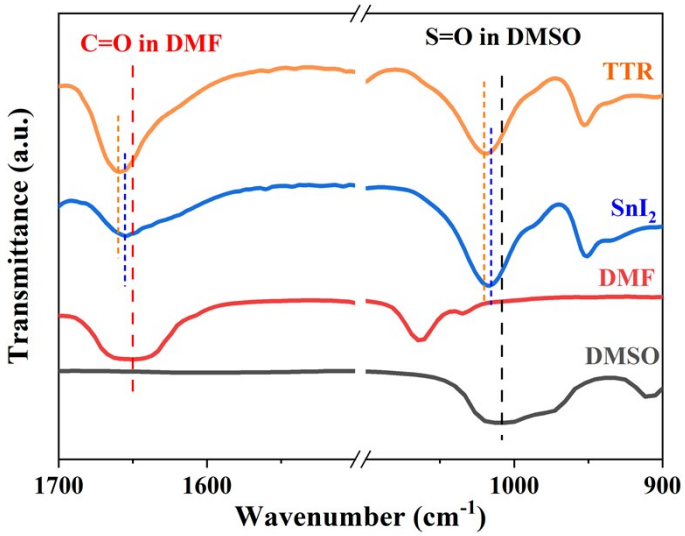

Figure S5. FTIR spectra of SnI_2 and TTR with DMSO/DMF.

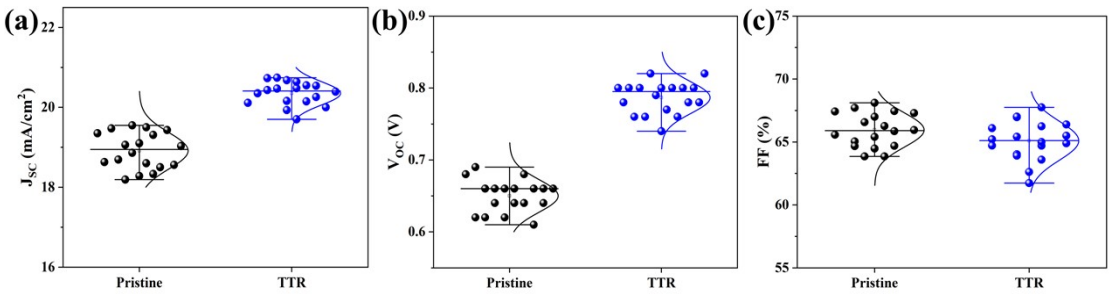

Figure S6. Box plot chart of a) J_{SC}, b) V_{OC} and c) FF of the pristine devices and TTR devices.

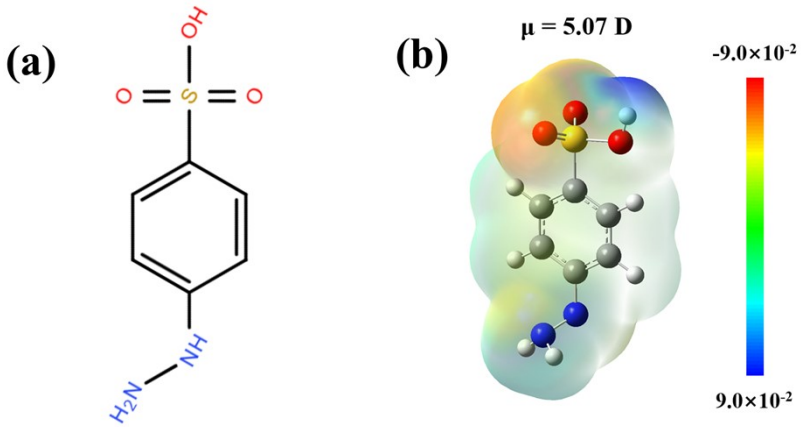

Figure S7. a) The Molecular structures of PHPA. b) The electrostatic potential (ESP) of PHPA.

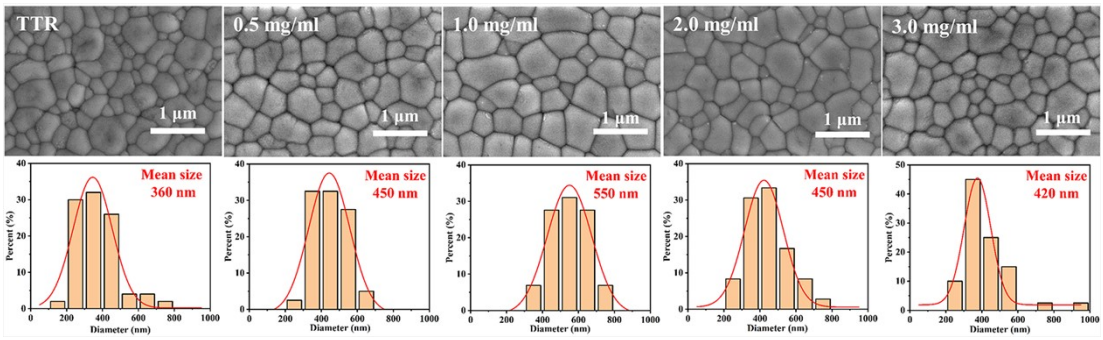

Figure S8. The SEM images and particle size distribution of TTR film with different addition concentrations of PHPA.

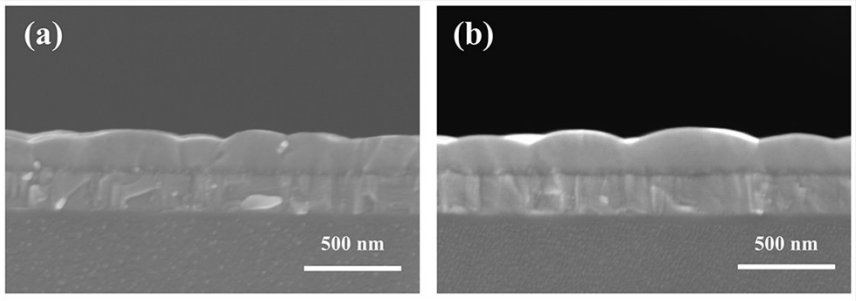

Figure S9. The cross-sectional SEM images of TTR film a) without and b) with PHPA.

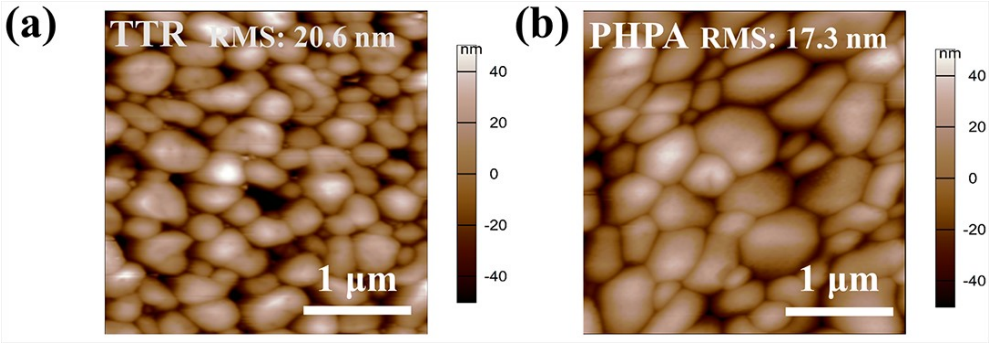

Figure S10. AFM measurements of TTR film a) without and b) with PHPA.

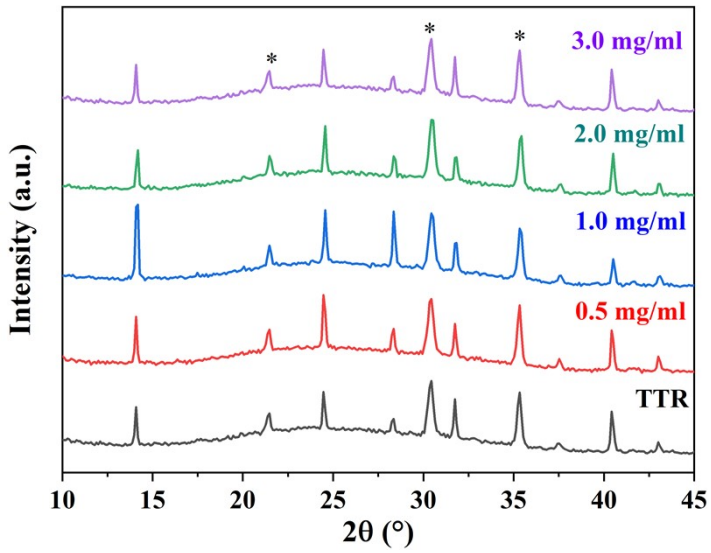

Figure S11. XRD patterns of TTR perovskite film with different addition concentrations of PHPA.

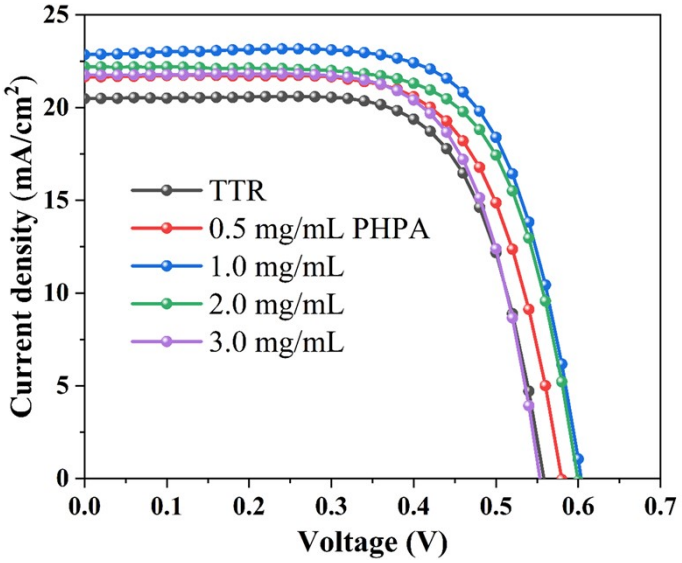

Figure S12. J-V curves of PSCs with different addition concentrations of PHPA using PCBM.

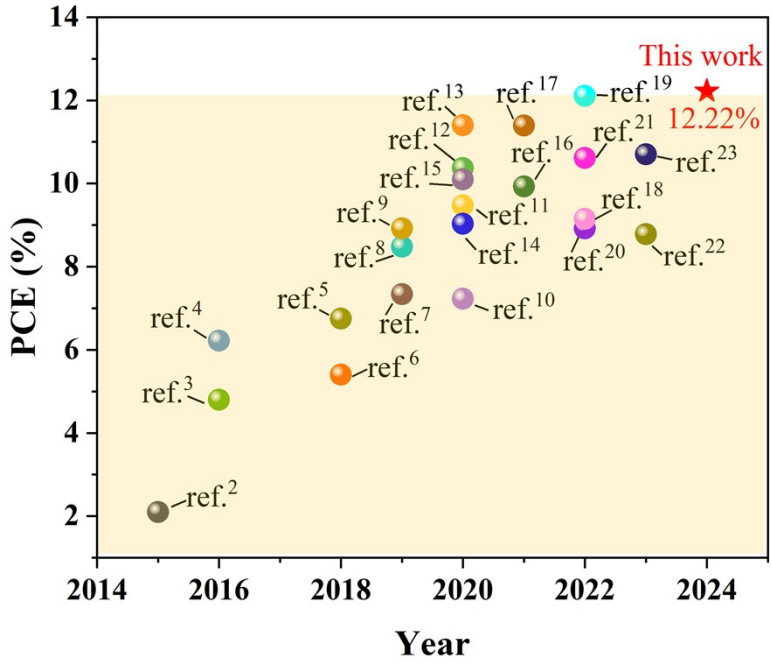

Figure S13. The efficiency development diagram of pure 3D $FASnI_3$ perovskite solar cells. [2-23]

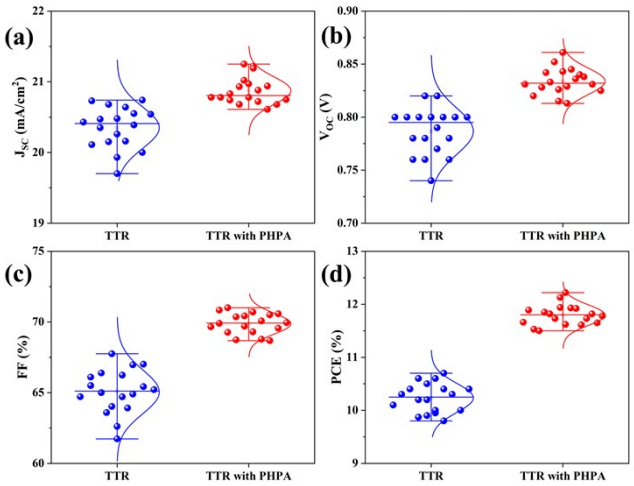

Figure S14. Statistic photovoltaic parameters of independent PSCs based on $FASnI_3$ films by the TTR and TTR with PHPA.

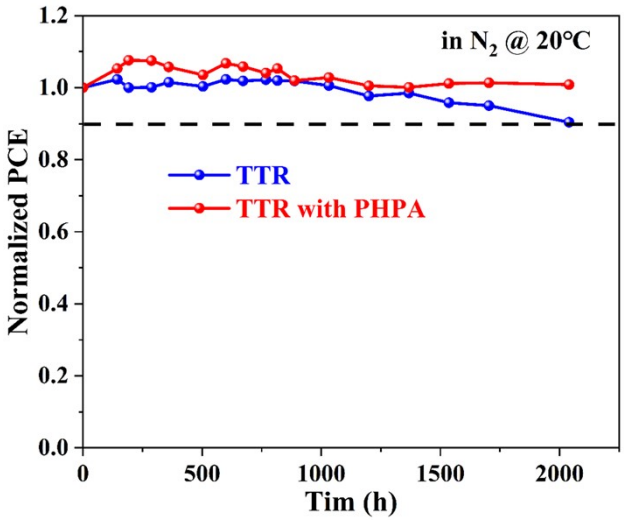

Figure S15. The long-term stability in N_2 under dack conditions for the TTR and PHPA devices

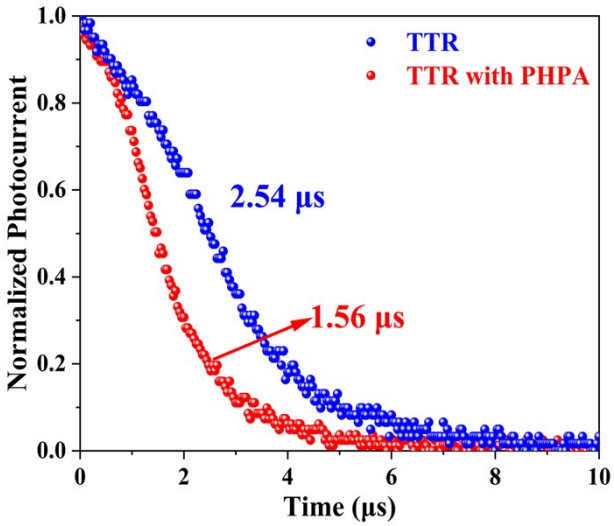

Figure S16. The TPC measurements of the TTR and PHPA perovskite devices.

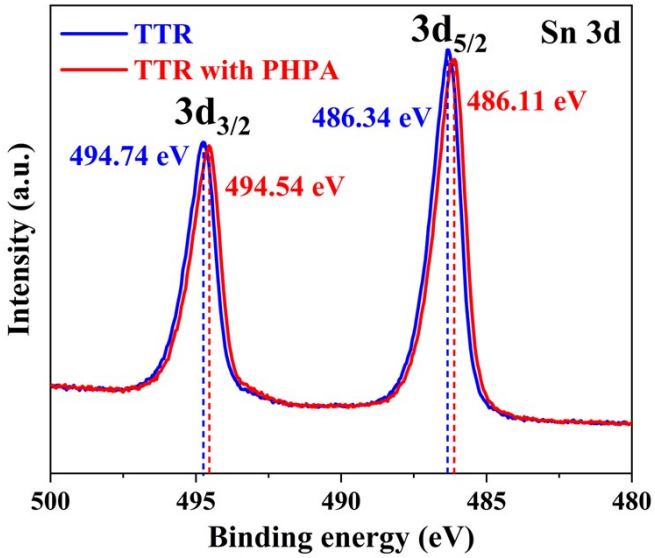

Figure S17. The XPS peaks of Sn 3d for the TTR and PHPA perovskite films.

Table S1. Contact angle (CA) and surface energy of different perovskite films.

Sn^{2+} source	Hexadecane CA (°)	Water CA (°)	Suface energy ($mJ \cdot m^{-2}$)		
			Dispersive Component	Polar Component	Total
SnI_2	6.3	55.1	27.43	21.06	48.49
TTR	12.0	70.3	27.00	11.68	38.68

Table S2. Standard potential of Tin element (Handbook of Chemistry and Physics, 2017).

Reaction	Potential (V)
$Sn^{2+} + 2\ e^- \rightarrow Sn\ (0)$	-0.1375
$Sn^{4+} + 2\ e^- \rightarrow Sn^{2+}$	+0.1510
$Sn^{4+} + 4\ e^- \rightarrow Sn\ (0)$	+0.0135

Table S3. The Fitting results of the TRPL spectra of TTR and PHPA perovskite films.

	A_1	τ_1(ns)	A_2	τ_2(ns)	R^2	τ_{ave}(ns)
TTR	0.9205	0.9278	0.1674	3.9941	0.9974	2.2742
PHPA	0.5166	1.7038	0.4842	5.5678	0.9996	4.6168

Table S4. The fitting results of XPS spectra for TTR and PHPA perovskite films.

		Sn $3d_{5/2}$		Sn $3d_{3/2}$		Sn^{2+} (%)	Sn^{4+} (%)
		Sn^{2+}	Sn^{4+}	Sn^{2+}	Sn^{4+}		
TTR	Position (eV)	486.0	486.7	494.4	495.2	75.83	24.17
	peak area	300895	95865	208354	66393		
PHPA	Position (eV)	486.1	486.8	494.5	495.3	88.40	11.60
	peak area	312650	41105	216530	28345		

Table S5. The detail data of the J-V curves of PSCs with PHPA using PCBM.

	J_{SC} (mA/cm^2)	V_{OC} (V)	FF (%)	PCE (%)
TTR	20.48	0.56	68.58	7.86
0.5 mg/ml	22.27	0.58	67.34	8.70
1.0 mg/ml	22.85	0.60	69.91	9.58
2.0 mg/ml	22.21	0.60	68.30	9.10
3.0 mg/ml	21.76	0.56	67.85	8.27

Table S6. Fitting parameters of PSCs from Nyquist plots.

	R_s (Ω)	R_{rec} (Ω)
TTR	14.4	1020
PHPA	15.1	3500

Reference

1. J.-W. Lee, D.-K. Lee, D.-N. Jeong and N.-G. Park, *Adv. Funct. Mater.*, 2019, **29**, 1807047.
2. T. M. Koh, T. Krishnamoorthy, N. Yantara, C. Shi, W. L. Leong, P. P. Boix, A. C. Grimsdale, S. G. Mhaisalkar and N. Mathews, *J. Mater. Chem. A*, 2015, **3**, 14996-15000.
3. S. J. Lee, S. S. Shin, Y. C. Kim, D. Kim, A. Tae Kyu, J. H. Noh, J. Seo and S. I. Seok, *J. Am. Chem. Soc.*, 2016, **138**, 3974-3977.
4. W. Liao, D. Zhao, Y. Yu, C. R. Grice, C. Wang, A. J. Cimaroli, P. Schulz, W. Meng, K. Zhu, R.-G. Xiong and Y. Yan, *Adv. Mater.*, 2016, **28**, 9333-9340.
5. F. Gu, S. Ye, Z. Zhao, H. Rao, Z. Liu, Z. Bian and C. Huang, *Sol. RRL*, 2018, **2**, 1800136.
6. M. E. Kayesh, T. H. Chowdhury, K. Matsuishi, R. Kaneko, S. Kazaoui, J.-J. Lee, T. Noda and A. Islam, *ACS Energy Lett.*, 2018, **3**, 1584-1589.
7. J. Cao, Q. Tai, P. You, G. Tang, T. Wang, N. Wang and F. Yan, *J. Mater. Chem. A*, 2019, **7**, 26580-26585.
8. F. Li, H. Fan, J. Zhang, J.-H. Huang, P. Wang, C. Gao, L.-M. Yang, Z. Zhu, A. K.-Y. Jen, Y. Song and K.-J. Jiang, *Sol. RRL*, 2019, **3**, 1900285.
9. X. Meng, J. Lin, X. Liu, X. He, Y. Wang, T. Noda, T. Wu, X. Yang and L. Han, *Adv. Mater.*, 2019, **31**, 1903721.
10. W. Gu, X. Xu, J. Chen, B. Ma, M. Qin, W. Zhu, J. Qian, Z. Qin, W. Shen, Y. Lu, W. Zhang, S. Chen, X. Lu and W. Huang, *Sol. RRL*, 2020, **4**, 2000153.
11. X. He, T. Wu, X. Liu, Y. Wang, X. Meng, J. Wu, T. Noda, X. Yang, Y. Moritomo, H. Segawa and L. Han, *J. Mater. Chem. A*, 2020, **8**, 2760-2768.
12. X. Meng, T. Wu, X. Liu, X. He, T. Noda, Y. Wang, H. Segawa and L. Han, *J. Phys. Chem. Lett.*, 2020, **11**, 2965-2971.
13. C. Wang, F. Gu, Z. Zhao, H. Rao, Y. Qiu, Z. Cai, G. Zhan, X. Li, B. Sun, X. Yu, B. Zhao, Z. Liu, Z. Bian and C. Huang, *Adv. Mater.*, 2020, **32**, 1907623.
14. T. Wang, Q. Tai, X. Guo, J. Cao, C.-K. Liu, N. Wang, D. Shen, Y. Zhu, C.-S. Lee and F. Yan, *ACS Energy Lett.*, 2020, **5**, 1741-1749.
15. T. Wu, X. Liu, X. He, Y. Wang, X. Meng, T. Noda, X. Yang and L. Han, *Sci. China Chem.*, 2020, **63**, 107-115.
16. Z. Dai, T. Lv, J. Barbaud, W. Tang, T. Wang, L. Qiao, H. Chen, R. Zheng, X. Yang and L. Han, *Sci. China Mater.*, 2021, **64**, 2645-2654.
17. X. Meng, Y. Li, Y. Qu, H. Chen, N. Jiang, M. Li, D.-J. Xue, J.-S. Hu, H. Huang and S. Yang, *Angew. Chem. Int. Ed.*, 2021, **60**, 3693-3698.
18. B. H. Chang, B. Li, Z. X. Wang, H. Li, L. Wang, L. Pan, Z. H. Li and L. W. Yin, *Adv. Funct. Mater.*, 2022, **32**, 2107710.
19. H. Jang, H. Y. Lim, Y. J. Yoon, J. Seo, C. B. Park, J. G. Son, J. W. Kim, Y. S. Shin, N. G. An, S. J. Choi, S. H. Kim, J. Jeong, Y. Jo, S. K. Kwak, D. S. Kim and J. Y. Kim, *Sol. RRL*, 2022, **6**, 2200789.
20. M. A. Karim, K. Matsuishi, T. H. Chowdhury, M. Abdel-Shakour, Y. He and A. Islam, *ACS Appl. Energy Mater.*, 2022, **5**, 15038-15047.
21. J. Sanchez-Diaz, R. S. Sánchez, S. Masi, M. Krecmarová, A. O. Alvarez, E. M. Barea, J. Rodriguez-Romero, V. S. Chirvony, J. F. Sánchez-Royo, J. P. Martinez-Pastor and I. Mora-Seró, *Joule*, 2022, **6**, 861-883.

22. J. Choi, S. J. Yang, S. G. Han, W. Sung, D. Yoo and K. Cho, *Chem. Mater.*, 2023, **35**, 1148-1158.
23. G. Zeng, D. Pu, L. Huang, H. Guan, S. Zhou, J. Zhou, W. Shen, G. Li, G. Fang and W. Ke, *J. Mater. Chem. A*, 2023, **11**, 11245-11253.